Session II

"Direct Mapping: The Last Frontier"

https://doi.org/10.1017/S0074180900083169 Published online by Cambridge University Press

INTERFEROMETRIC IMAGING OF STELLAR SURFACES

D. MOZURKEWICH
U. S. Naval Research Laboratory
Remote Sensing Division
4555 Overlook Avenue, SE
Washington, DC 02375-5351, U.S.A.

Abstract.

Until recently, all study of stellar surface structure, except for the sun, has been limited to indirect methods. This state of affairs is rapidly changing. With the introduction of interferometric techniques to optical astronomy, direct imaging of stellar surfaces is finally possible. Within a few years we will have images with sub-milliarcsecond resolution and 10 or more resolution elements across the stellar surface.

In this talk, I will describe the technique of optical interferometry and explain how it can be made to work through the earth's turbulent atmosphere. I will show some actual data and describe what can be expected in the near future.

1. Introduction

The history of optical interferometry goes back more than a century, but only in the past decade has it become possible to compensate for atmospheric turbulence well enough to generate the high quality and volume of data needed to make images with an interferometer. Figure 1 (taken from Quirrenbach et al. (1994)) indicates the imaging capabilities that are becoming available at optical wavelengths. The left panel of Figure 1 is an image of circumstellar gas surrounding ζ Tauri taken in Hα light with the Mark III Stellar Interferometer on Mt. Wilson. The resolution, shown by the beam profile in right panel, is about 2 milliarcseconds (mas) north-south and 4 mas east-west.

There are many groups doing this type of work with many variants of the technique (Armstrong et al. (1995)); this talk is biased toward the project I am most familiar with, a collaboration between the US Naval Research

K. G. Strassmeier and J. L. Linsky (eds.), Stellar Surface Structure, 131–138.

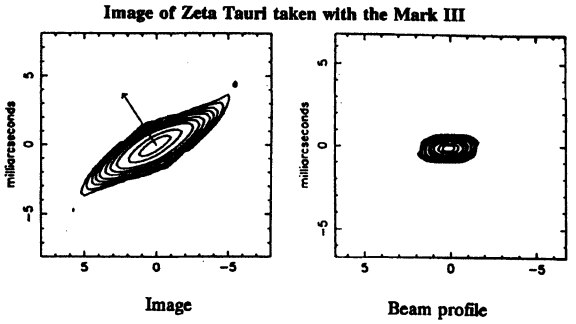

Figure 1. This figure shows the hydrogen disk surrounding the Be star ζ Tauri. This image was made in H α light. Images with similar resolution at optical wavelengths will soon be common.

Laboratory and the US Naval Observatory. In collaboration with CfA and MIT, we built the Mark III Optical Interferometer on Mount Wilson, CA, USA (Shao et al. (1988)). We operated that instrument from 1986 until 1992, when it was decommissioned so that we could concentrate our efforts on its successor, the Navy Prototype Optical Interferometer (NPOI). The NPOI is being built in collaboration with Lowell Observatory and is located on Anderson Mesa, southeast of Flagstaff, AZ, USA.

2. How optical interferometry works

An interferometer coherently brings together two separated sections of the wavefront. A schematic layout of a simple, two-element interferometer is shown in Figure 2. The afocal telescopes intercept sections of the wavefront and direct them toward the beam combiner. Because the light is not monochromatic, portions of the same wavefront intercepted by the telescopes must arrive at the beam combiner simultaneously. In order to accomplish this, we must insert a variable delay into the path from at least one of the telescopes. The delay can be thought of either as a time or as the distance light travels during that time. I will switch between these two usages. The variable delay is added to the optical path with delay lines, which consist of retroreflectors mounted on tracks. The delay lines at the NPOI can track fringes moving at 2 cm/sec with a root mean square error of less then 20 nm. They have a range of 35 meters of optical path.

Because we are using relatively narrow bandpasses centered on the fringe packet and are only concerned with small excursions in delay, we can assume the system response to a point source is a sinusoidal function of delay. The quantities that we measure are the amplitude and the phase of this interference fringe. To see how these are related to the intensity distribution

https://doi.org/10.1017/S0074180900083169 Published online by Cambridge University Press

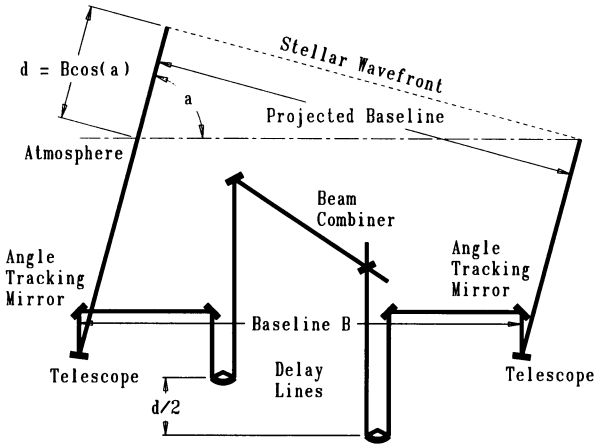

Figure 2. A two-element Michelson interferometer. The layout shown here is that of the Mark III Optical Interferometer on Mt. Wilson.

of the source, consider Figure 3. The delay lines are set to remove the delay between telescopes for the direction of the solid lines. The portion of the source in the direction of the dotted lines gives rise to a fringe whose amplitude is proportional to the intensity in that direction and whose phase is delayed by $B_\perp\theta$, where $B_\perp$ is the component of B perpendicular to the direction of the star. We convert the delay to a phase by changing from units of length to units of radians of a fringe, and we integrate over all angles in the source to get the system response

$$V = \int I(\theta)\ exp[2\pi i(\frac{B_\perp}{\lambda})\theta]d\theta.$$

V is a complex number whose amplitude and phase are the amplitude and phase of the fringe. If V is normalized by the total flux, it is refered to as the visibility. This equation shows that V is also the Fourier transform of the source brightness distribution, $I(\theta)$, evaluated at the projected baseline vector $B_\perp/\lambda$.

If we do not measure enough Fourier components from one observation of the source to make an image, we can improve our coverage either by moving the telescopes or by waiting for the earth to rotate, changing the projected baseline. This later approach—called earth-rotation synthesis—has been successfully employed by astronomers using interferometers from radio to optical wavelengths.

As an example of how this works in practice, we present the data from one night's observation of α Equulei, a previously unresolved spectroscopic

https://doi.org/10.1017/S0074180900083169 Published online by Cambridge University Press

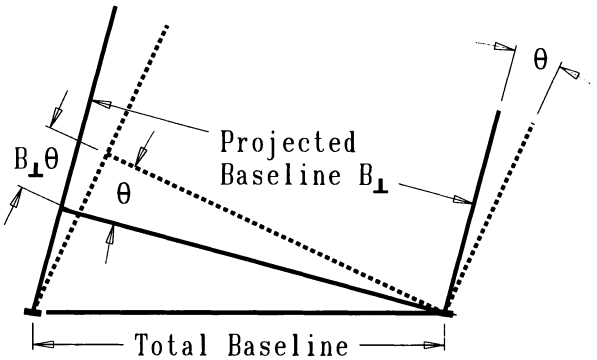

Figure 3. A two-element interferometer observing flux coming from two directions on the sky (indicated by solid and dashed lines, respectively).

binary star (Armstrong et al. (1992)). The left panel of Figure 4 shows the variation of fringe amplitude with time at three wavelengths. To interpret this data, we calculated the projected baseline for each observation (measured in wavelengths) and plotted those points in the right panel. North is up and east is to the right, so that time progresses from left to right across the top of the figure. Larger visibility amplitudes are plotted with larger circles.

We have two more pieces of information. First, Equation 1 tells us that there is a maximum at the origin. Second, for a real (i.e. not complex) brightness distribution, the amplitudes of the Fourier transform are unchanged on a reflection through the origin. This means we can plot each of the data points a second time, in the bottom half of the figure.

We now see that all the maxima can be fit by assuming they lie on parallel, equally spaced lines. If we further assume that the amplitude varies sinusoidally between the lines, we get the fit to the data shown as the solid lines in left panel of figure 4. The fringe amplitude does not vary in the direction along the lines, so the source is unresolved in that direction, since the Fourier transform of a delta function is a constant. The fringe amplitude varies sinusoidally in the direction perpendicular to the lines, so we are observing a binary star, since the Fourier transform of a pair of delta functions is a sinusoid. The separation of the stars in radians is equal to the inverse of the spacing of the maxima. Measuring the separation of these lines gives a separation for the stars of 11 mas.

3. Atmospheric limitations

Atmospheric turbulence distorts and delays the wavefront arriving from a star. This distortion varies with time and position. In order for the interfer-

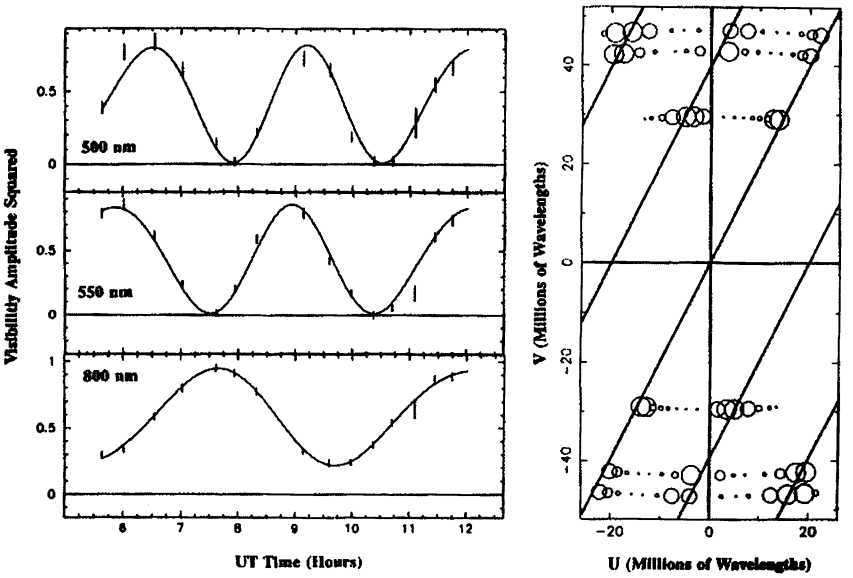

Figure 4. Interferometric data of the spectroscopic binary α Equulei plotted as functions of time and projected baseline.

ometer to work, a coherent integration time has to be chosen short enough to freeze the turbulence, and the aperture size has to be small enough so that the wavefront is locally flat. These limits are referred to as the coherence time, t_0, and the coherence length, r_0. The coherence time is typically a few milliseconds, and the coherence length, often referred to as Fried's parameter, is typically 5 to 20 cm.

To carry out an interferometric observation under these conditions, we first intercept locally flat segments of the wavefront with two or more telescopes. These segments must then be made parallel to one another and perpendicular to the optical axis of the instrument. This angle tracking is accomplished by superposing the images with a fast tip-tilt mirror at each telescope. Finally, after combining the beams, we measure the fringe phase to determine the difference in arrival time of the segments, and adjust the delay so that segments of subsequent wavefronts arrive simultaneously. As long as we do a reasonably good job of superposing the images and correcting the delays, we obtain good fringe amplitude information on each baseline. Observing stars of small angular diameter allows us to calibrate the instrumental response and generate reliable calibrated amplitudes.

The effect of the atmosphere on the fringe phases is more severe than on the amplitudes. A typical plot of atmospherically-induced delay versus time is shown in Figure 5. The peak-to-peak fringe motion is roughly 10

https://doi.org/10.1017/S0074180900083169 Published online by Cambridge University Press

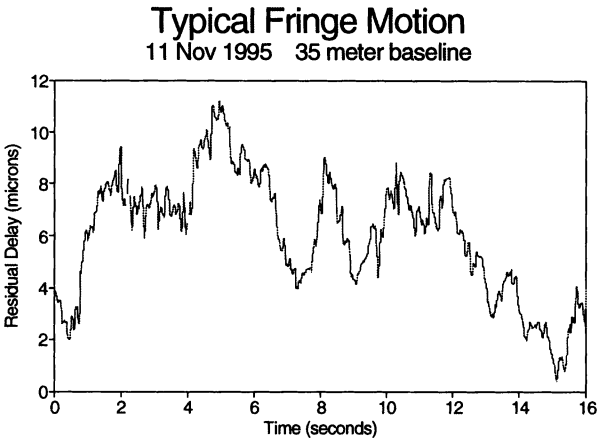

Figure 5. Delay variations due to atmospheric turbulence plotted vs. time. These data were taken with the NPOI.

μm, or 40π radians at a wavelength of 0.5 μm. Clearly, even if we have succeeded in tracking this motion, we have lost any information carried by the phases.

To get around this problem, we note that even though the individual phases are corrupted by the atmosphere, there are combinations of the observed phases that are not affected by the atmosphere. These phase-like quantities are formed by summing the phases around closed loops and are therefore called "closure phases". For example, consider three elements of an interferometer labeled A, B and C. The delay measured on baseline (A-B) is defined as the time of arrival of the wavefront at element B minus the time of arrival at element A. We observe fringes simultaneously on baselines (A-B), (B-C), and (C-A). The closure phase formed by adding these three phases is independent of the atmosphere. When atmosphere is added over element B, for instance, the arrival of the wavefront at element B is delayed. The delay measured on baseline (A-B) is increased by exactly the same amount as the delay on baseline (B-C) is decreased, leaving the closure phase unaffected.

The use of closure phases, pioneered by radio VLBI observers, allows us to recover a substantial amount of the lost fringe phase information. With N interferometer array elements, we have $N(N-1)/2$ baselines, each with a measured delay. These delays have been corrupted by the atmosphere, which introduces unknown retardations of the wavefront at each of the N telescopes. We are free to subtract a constant delay (*e.g.*, the mean value) from each individual delay, which corresponds to a shift of the image on the sky. Thus, there are only $(N-1)$ quantities that distort the image. This

leaves $N(N-1)/2-(N-1) = (N-1)(N-2)/2$ "good phases"–quantities that retain information about the image structure. The ratio of the number of "good phases" to the $N(N-1)/2$ phases available in the absence of the atmosphere quickly reaches a reasonable fraction as N increases.

With these techniques, the atmosphere does not limit the quality of the fringe data. Good angle and delay tracking gives good amplitude measurements, and using several telescopes simultaneously recovers most of the phase information. So the main effect of the atmosphere on an interferometer–aside from increasing its complexity–is that the combination of t_0 and r_0 puts a limit on its sensitivity: we must gather enough photons to make it possible to detect the fringe within t_0 with two apertures of size r_0.

4. Limits of resolution

The resolution of an optical interferometer is determined by the maximum baseline length, which is limited by the available real estate and the cost of the delay lines. To date, the longest baseline planned is 600 m at the Sydney University Stellar Interferometer, located near Narrabri, NSW, Australia. The resulting resolution (λ/B, where B is the baseline length) is about 0.15 mas at optical wavelengths. Interferometers built on mountaintops, where the seeing is expected to be better, will have shorter baselines whose lengths are limited by the topography.

However, unlike the case of radio interferometers, there is also a limit to the number of resolution elements across the image. We have to know the delay of the fringe in order to measure the fringe parameters. For bright stars observed on short baselines, this is not a problem. We simply detect the fringe using an integration time shorter than the atmospheric coherence time. The signal to noise goes as NV^2, where N is the number of photons detected during the coherent integration time. N is fixed by the choice of star and the size of the telescopes. As the baseline is lengthened the star becomes resolved and the visibility amplitude drops. The resolution is limited to that obtained from the longest baseline with a signal to noise above the fringe tracking threshold. Using a single baseline, we can get only a few resolution elements across the star.

This is not a fundamental limit. The number of resolution elements can be increased by observing objects that have very small, bright spots embeded in a much larger structure. The emission region surrounding a Be star, like ζ Tauri, is a good example of this type of object. Another possibility is to build up a long baseline out of several shorter ones. The fringe delay on each of the short baselines determines the delay on the long baseline. This approach was built into the NPOI design. Finally, we can build larger telescopes with adaptive optics to increase the number of

photons detected per coherence time. Note that although adaptive optics can be used to increase the resolution of an optical interferometer, it is of limited use for improving the sensitivity since an unresolved star that is bright enough for an adaptive optics system is also bright enough for the fringe detector.

With the interferometers currently built or under construction, we will be limited to about 10 resolution elements across the diameter of a featureless star. Even so, the interferometric images will be comparable to much of what is being presented at this conference.

Finally, the capabilities of the NPOI are presented in Table 2. The first column presents what is either currently available. The second column shows what we expect a few years down the road.

TABLE 1. Current and projected capabilities of the NPOI.

	Current	Near future
Sensitivity	$m_V = 6.0$	$m_V = 8.0 - 10.0$
Resolution	3 mas	0.2 mas
Wavelength coverage	450 – 850 nm	also 2 μm
Resolution elements across star	3	15

Acknowledgements: Basic research in Infrared and Optical Interferometry at the Naval Research Laboratory is supported by the Office of Naval Research through funding document number N00014-93-WX-35012, under NRL work unit 1798. I would like to thank J. T. Armstrong and T. A. Pauls for help in preparing this paper.

References

Armstrong, J.T., Hutter, D.J., Johnston, K.J. and Mozurkewich, D. (1995) *Physics Today*, **48(5)**, pp.42-49

Armstrong, J.T., Mozurkewich, D., Vivekanand, M., Simon, R.S., Denison, C.S., Johnston, K.J., Pan, X.-P., Shao, M., and Colavita, M.M. (1992) *AJ*, **104**, 241

Quirrenbach, A., Buscher, D.F., Mozurkewich, D., Hummel, C.A., and Armstrong, J.T. (1994) *A&A*, **203**, L13

Shao, M., Colavita, M.M., Hines, B.E., Staelin, D.H., Johnston, K.J., Mozurkewich, D., Simon, R.S., Hershey, J.L., and Kaplan, G.H. (1988) *A&A*, **193**, 357